Large-Scale Synthesis and Characterization of Helically Coiled Carbon Nanotubes by Use of $Fe(CO)_5$ as Floating Catalyst Precursor

Haoqing Hou,* Zeng Jun, Frank Weller, and Andreas Greiner

Department of Chemistry and Materials Science Center, Philipps University Marburg, Hans-Meerwein Strasse, D-35032 Marburg, Germany

Received August 16, 2002. Revised Manuscript Received January 29, 2003

Helically shaped multiwalled carbon nanotubes (HCNTs) (diameter 30−80 nm) were obtained as main products in large quantities by co-pyrolysis of $Fe(CO)_5$ as floating catalyst precursor and pyridine or toluene as carbon source at temperatures above 1000 °C under flow of hydrogen. In contrast, pyrolysis at 700−800 °C yielded only carbon-coated Fe nanoparticles. The HCNTs were characterized by electron microscopy, Raman spectroscopy, and wide-angle X-ray diffraction. The growth mechanism of the HCNTs was discussed on the basis of previously reported models.

1. Introduction

Carbon nanotubes have gained significant interest since their pioneering discovery by Ijima.[1] Carbon nanotubes are known as multiwalled (MWNT) or single-walled carbon nanotubes (SWNT).[2] Besides cylindrical carbon nanotubes, different shapes have been observed for carbon nanotubes, including helically coiled carbon nanotubes (HCNTs), which are shown in Figure 1. HCNTs were predicated in the early 1990s[3−6] and were observed experimentally in 1994.[7−8] According to computer simulation with molecular dynamics calculations, HCNTs are energetically and thermodynamically stable. The coiling mechanism of HCNTs attracted the interest of scientists in the following several years.[8−15] It was proposed in those studies that curving and coiling could be accomplished by the occurrence of "knees" connecting two straight cylindrical tube sections of the same diameter. Such knees can be obtained via the insertion in the plane of the knee of diametrically opposed pentagonal (C_5) and heptagonal (C_7) carbon rings in the hexagonal (C_6) network. The heptagon with its negative curvature is on the inner side of the knee and the pentagon is on the outer side (see Figure 1A).

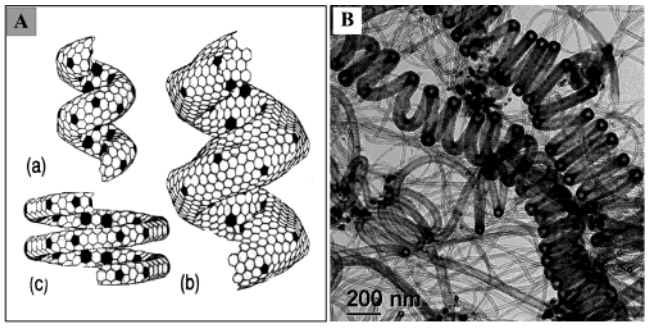

Figure 1. (A) Scheme (reproduced with permission from ref 5) of the helical cage forms of carbon that have the lowest cohesive energy per atom (only two pitch lengths are shown): (a) helix C_{360}, (b) helix C_{1080}, and (c) helix C_{540}. The C_5 and C_7 rings (shaded) appear in the outer and inner ridgelines, respectively, amid a background of the C_6 rings. (B) TEM image of multiwalled helically coiled carbon nanotubes produced by the pyrolysis of vapor mixture of $Fe(CO)_5$ and pyridine under a H_2 flow at 1050−1150 °C.

A study of the electronic structure of HCNTs by Akagi et al.[16] showed that an HCNT could be (1) a metal, (2) a semiconductor, or (3) a semi-metal depending on the position of the pentagon and of the heptagon after folding the energy bands of the constituent carbon nanotubes. On the basis of their calculations, the authors conclusively mentioned that HCNTs could be candidates for superconductors because of the sharp peak of the corresponding densities of states (DOS) of HCNTs at the Fermi level.

To the best of our knowledge, no breakthrough has been made in the preparation of HCNTs that compares

* To whom correspondence should be addressed at Department of Polymer Science, University of Akron, Akron, Ohio, 44325-3909. Telephone: 330-972-8615. Fax: 330-972-5290. E-mail: haoqing@uakron.edu.

(1) Iijma, S. *Nature* **1991**, *354*, 56.
(2) Huczko, A. *Appl. Phys. A* **2002**, *74*, 617.
(3) Dunlap, B. I. *Phys. Rev. B* **1992**, *46*, 1933.
(4) Itoh, S.; Ihara, S.; Kitakami, J. *Phys. Rev. B* **1993**, *47*, 1703.
(5) Itoh, S.; Ihara, S.; Kitakami, J. *Phys. Rev. B* **1993**, *48*, 5643.
(6) Itoh, S.; Ihara, S. *Phys. Rev. B* **1993**, *48*, 8323.
(7) Ivanov, V.; Nagy, J. B.; Lambin, Ph.; Lucas, A. A.; Zhang, X. B.; Zhang, X. F.; Bernaerts, D.; Tendeloo, G. Van; Amelinckx, S.; Landuyt, J. Van *Chem. Phys. Lett.* **1994**, *223*, 329.
(8) Zhang, X. B.; Zhang, X. F.; Bernaerts, D.; Tendeloo, G. Van; Amelinckx, S.; Landuyt, J. Van; Ivanov, V.; Nagy, J. B.; Lambin, Ph.; Lucas, A. A. *Europhys. Lett.* **1994**, *27*, 141.
(9) Bernaerts, D.; Zhang, X. B.; Zhang, X. F.; Tendeloo, G. Van; Amelinckx, S.; Landuyt, J. Van; Ivanov, V.; Nagy, J. B. *Philos. Mag.* **1995**, *71*, 605.
(10) Amelinckx, S.; Zhang, X. B.; Bernaerts, D.; Zhang, X. F.; Ivanov, V.; Nagy, J. B. *Science* **1994**, *265*, 635.
(11) Weaver, J. H. *Science* **1994**, *265*, 511.
(12) Fonseca, A.; Hernadi, K.; Nagy, J. B.; Lambin, Ph.; Lucas, A. A. *Carbon* **1995**, *33*, 1759.
(13) Ihara, S.; Itoh, S. *Carbon* **1995**, *33*, 931.
(14) Setton, R.; Setton, N. *Carbon* **1997**, *35*, 497.
(15) Fonseca, A.; Hernadi, K.; Nagy, J. B.; Lambin, Ph.; Lucas, A. A. *Synth. Met.* **1996**, *77*, 235.
(16) Akagi, K.; Tamura, R.; Tsukada, M. *Phys. Rev. Lett.* **1995**, *74*, 2307.

10.1021/cm021290g CCC: $25.00
Published on Web 07/08/2003

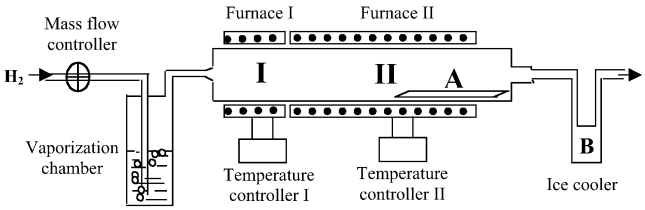

Figure 2. Schematic diagram of the apparatus used for the synthesis of HCNTs.

to the progress in the large-scale synthesis of SWNTs[17] or MWNTs.[18] Several contributions reported the synthesis of HCNTs[7−8,19−21] by chemical vapor deposition (CVD) on preformed substrates.[2] HCNTs were obtained as byproducts of MWNTs. Co−silica or Fe−silica catalysts were prepared as preformed substrates, which served as substrates for the preparation of HCNTs by catalytic pyrolysis of acetylene. The selectivity of the formation of HCNTs was optimized for the Co−silica or Fe−silica catalysts by modification of the reaction conditions.[19,21] HCNTs were also found as low-content byproducts of MWNTs in microwave plasma-enhanced CVD (MW-PECVD) synthesis[22] as well as in CVD using floating catalyst synthesis.[23]

$Fe(CO)_5$ was reported as a very effective floating catalyst precursor for the formation of SWNTs[17,24] and MWNTs[25] in large scale or even for the preparation of metal nanoparticles.[26] In this paper we present the pyrolytic large-scale synthesis and characterization of HCNTs using $Fe(CO)_5$ as a floating catalyst precursor.

2. Experimental Section

Materials. Hydrogen (Messer), $Fe(CO)_5$ (99.99%, Aldrich), pyridine (99%, Aldrich), and toluene (99%, Aldrich) were used as received. Silicon wafers (both sides polished, Wacker Siltronic) were cut into 3 × 6 cm slide pieces and washed with acetone 2× before use.

Synthesis Apparatus. The experimental setup, depicted schematically in Figure 2, is identical to the equipment reported previously.[27] The apparatus is composed of a vaporization chamber, two pyrolysis zones, and an ice cooler. The pyrolysis zone was equipped with a dual furnace fitted with independent temperature controllers and a quartz glass tube (3.5 cm i.d., length 95 cm, heating length 65 cm).

HCNTs Synthesis. One gram of $Fe(CO)_5$ was dissolved into 99 g of pyridine to obtain a feed solution with 1 wt % $Fe(CO)_5$.

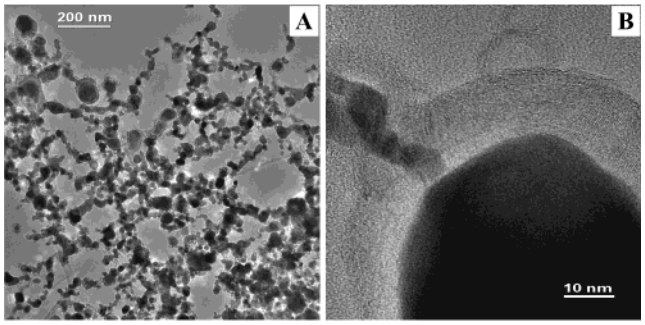

Figure 3. Low (A) and high (B) magnification TEM images of the pyrolysis product of the vapor mixture of pyridine and $Fe(CO)_5$ at 700−800 °C.

Table 1. Operating Conditions for the Preparation of HCNTs by Pyrolysis of Vapor Mixture of $Fe(CO)_5$ and Pyridine or Toluene

run	$Fe(CO)_5$ solvent (1/99)	temperature of pyrolysis (°C)	reaction time (min)	yield (mg)	trait of product	size (ϕ nm)
A	pyridine	700−800	150	324	nanoparticles	20−100
B	pyridine	1050−1150	240	1079	HCNTs	30−80
C	toluene	1050−1150	240	870	HCNTs	30−80

The solution was fed into the vaporization chamber. A H_2 flow of 350−400 mL/min was introduced into the solution. The vapor mixture of pyridine and $Fe(CO)_5$ was carried by the stream of H_2 into the two-stage tubular quartz reactor. The pyrolysis of the vapor mixture was performed in H_2 atmosphere at 1050−1150 °C. The resulting HCNTs were precipitated both on the silicon substrate and on the wall of the quartz tube as a black layer, which could be scraped off from the silicon and quartz substrate as some mat-like lumps. The resulting product was washed with CS_2 in an ultrasonic bath 2× and dried at 100 °C under vacuum for 12 h. The pyrolysis reaction parameters, yields, and some features are listed in Table 1.

Measurements. Scanning electron microscopy (SEM) images of the resulting products were obtained using a Cam Scan 4 microscope operated at 15 kV accelerating voltage. The SEM samples were prepared by attaching a small piece of the black mat-like lump to a SEM sample holder through a conductive sticking tape. A layer of Au about 5 nm thick was coated onto the sample surface using an Edwards AUTO 306 coating system. Transmission electron microscopy (TEM) images were obtained using a JEM 3010 microscope operated at 300 kV. A small amount of the above resulting product was dispersed in 20 mL of $CHCl_3$ using an ultrasonic bath and loaded onto a Cu-grid TEM sample holder. Raman spectroscopy was performed using a Jobin-Yvon LABRAM HR800 with 514.5-nm Ar laser excitation. Wide-angle X-ray scattering (WAXS) was performed with a Siemens D5000 using Cu α radiation.

3. Results and Discussion

3.1. Synthesis of HCNTs by CVD Pyrolysis. Only carbon-coated nanoparticles were obtained when the vapor mixture of pyridine and $Fe(CO)_5$ was decomposed in reducing atmosphere H_2 (gas flow rate 350−400 sccm) at 700−800 °C (Table 1, run A; Figure 3).

The resulting products were mainly HCNTs when the pyrolysis of the vapor mixture of $Fe(CO)_5$ and pyridine or toluene was performed at 1050−1150 °C (Table 1, run B or run C). Inspection by SEM and TEM (Figure 4) revealed that the resulting product was composed of mainly multiwalled HCNTs, with different helix diameters and different helix pitch heights, which grew either on the silicon substrate or on the wall of the quartz tube.

(17) Nikolaev, P.; Bronikowski, M. J.; Bradley, R. K.; Fohmund, F.; Colbert, D. T.; Smith, K. A.; Smalley, R. E. *Chem. Phys. Lett.* **1999**, *313*, 91.
(18) Andrews, R.; Jacques, D.; Rao, A. M.; Derbyshire, F.; Qian, D.; Fan, X.; Dickey, E. C.; Chen, J. *Chem. Phys. Lett.* **1999**, *303*, 467.
(19) Piedigrosso, P.; Konya, Z.; Colomer, J.; Fonseca, A.; Tendeloo, G. V.; Nagy, J. B. *Phys. Chem. Chem. Phys.* **2000**, *2*, 163.
(20) Ivanov, V.; Fonseca, A.; Nasy, J. B.; Lucas, A.; Lambin, P.; Bernaerts, D.; Zhang, X. B. *Carbon* **1995**, *33*, 1727.
(21) Hernadi, K.; Fonseca, A.; Nagy, J. B.; Bernaerts, D.; Lucas, A. A. *Carbon* **1996**, *34*, 1249.
(22) Wang, X.; Hu, Z,; Wu, Q.; Chen, X.; Chen, Y. *Thin Solid Films* **2001**, *390*, 130.
(23) Sen, R.; Govindaraj, A.; Rao, C. N. R. *Chem. Mater.* **1997**, *9*, 2078.
(24) Satishkumar, B. C.; Govindaraj, A.; Sen, R.; Rao, C. N. R. *Chem. Phys. Lett.* **1998**, *293*, 47.
(25) Rohmund, F.; Falk, L. K. L.; Campbell, E. E. B. *Chem. Phys. Lett.* **2000**, *328*, 369.
(26) Li, Y. Liu, J. Wang, Y.; Wang, Z. L. *Chem. Mater.* **2001**, *13*, 1008.
(27) Schäfer, O.; Greiner, A.; Pommerehne, J.; Guss, W.; Vestweber, H.; Tak, H. Y.; Bässler, C.; Schmidt, C.; Lüssem, G.; Schartel, B.; Stümpflen, V.; Wendorff, J. H.; Spiegel, S.; Moeller, C.; Spiess, H. W. *Synth. Met.* **1996**, *82*, 1.

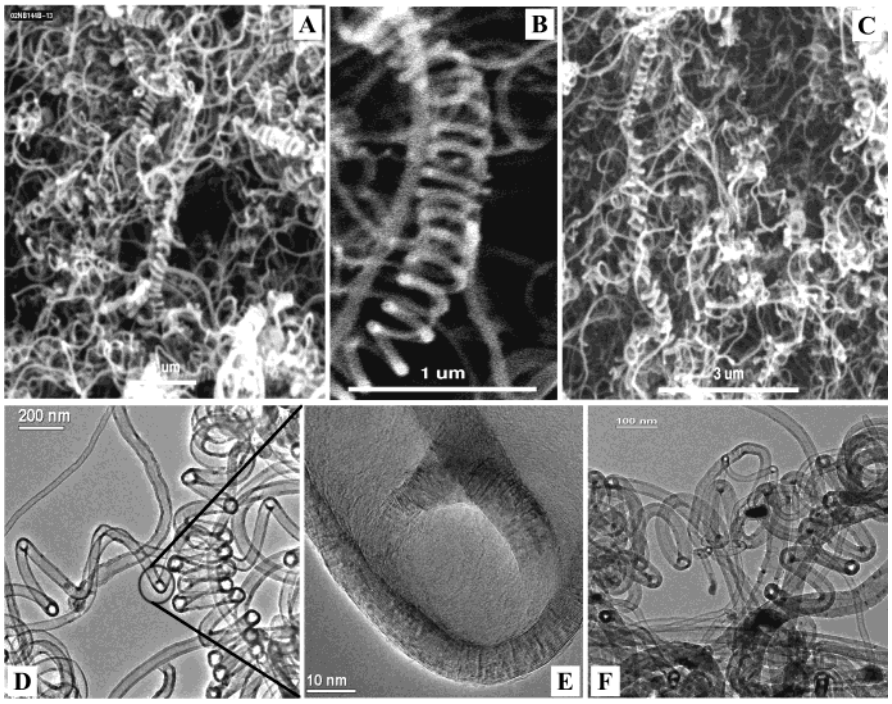

Figure 4. A and B, SEM images, and D and E, TEM images, of HCNTs formed by pyrolysis of vapor mixture of pyridine and $Fe(CO)_5$ in H_2 atmosphere at 1050−1150 °C. C and F, respectively, SEM and TEM graphs of the product of run C produced by using toluene as carbon source.

Amorphous carbon fibers containing iron particles were reported for the pyrolysis of pure $Fe(CO)_5$ in a reducing atmosphere at 900 °C.[23] However, the pyrolysis of a gas mixture of C_2H_2 and $Fe(CO)_5$ resulted in SWNTs at 1100 °C[24] and large-scale aligned MWNTs at 750 °C (with H_2).[25] The pyrolysis of a gas mixture of CO and $Fe(CO)_5$ yielded SWNTs in a wide temperature range from 850 to 1200 °C.[17] In our experiments, pyridine or toluene was used as an additional carbon source for the formation of carbon nanotubes. The formation of carbon-coated nanoparticles at lower temperatures (run A) is most likely due to the fact that pyridine rings are stable under these conditions and do not liberate C_n carbon species[28] for the formation of carbon tubular structures.

3.2. Raman Spectra Analysis. According to Thomsen's studies,[29] it is reasonable to believe that the inner (more strongly curved) tubes of a MWNT contribute to the SWNT-like feature observed in Raman spectra, whereas the outer tubes more closely resemble graphite. The recent reports[30,31] on radial breathing mode (RBM) of MWNTs further approved Thomsen's studies. When the diameters of the inner tubes are small enough to be the same order as that of the SWNTs, the MWNTs perhaps give rise to the appearance of the breathing modes of MWNTs, similar to those of the SWNTs.[32] In our case, though the HCNTs are multiwalled helically coiled carbon nanotubes, the diameters of the inner tubes are far from the order of the diameter of SWNTs (see Figure 4), and no RBM peak should be observed. The low-frequency peaks shown in Figure 5 should not be the RBM of the MWNTs or SWNTs. No SWNTs were found in the samples by 5× repeated sampling and observation using transmission electron microscope. Compared with the Raman spectra of Fe_2O_3 (see the insert of Figure 5) and literature reports,[33−34] we found that these low-frequency peaks could be assigned to the contribution of iron oxide (Fe_2O_3) impurity in the sample due to the air oxidation of iron nanoparticles that were formed during the synthesis process of HCNTs.

As shown in Figure 5, the first-order modes of the Raman spectra of the HCNTs show a strong sharp peak at 1577.7 cm^{-1} (G line), which can be assigned to the high-frequency E_{2g} first-order mode, and a strong sharp peak at 1349.9 cm^{-1} (D line) as well as a weak peak, appeared as a shoulder peak of G line, at 1612.9 cm^{-1} (D′ line). The origin of the D and D′ lines has been explained as disorder-induced features due to the finite particle size effect or lattice distortion of graphite crystals.[35−37] Therefore, the very strong relative intensity of the D line (in Figure 5) may be the result of a high lattice distortion of graphite crystals in the HCNTs. The weak peak at 1099.0 cm^{-1} was rarely reported previously. Li et al.[38] reported a weak peak at 1094 cm^{-1}

(28) Li, D. C.; Dai, L.; Huang, S.; Mau, A. W. H.; Wang, Z. L. *Chem. Phys. Lett.* **2000**, *316*, 349.
(29) Thomsen, C. *Phys. Rev. B* **2000**, *61* (7), 4542.
(30) Ando, Y.; Zhao, X.; Shimoyama, H.; Sakai, G.; Kaneto, K. *Int. J. Inorg. Mater.* **1999**, *1*, 77.
(31) Zhao, X.; Ando, Y.; Qin, L.-C.; Kataura, H.; Maniwa, Y.; Saito, R. *Physica B* **2002**, *323*, 265.
(32) Rao, A. M.; Richter, E.; Bandow, S.; Chase, B.; Eklund, P. C.; Williams, K. A.; Fang, S.; Subbaswamy, K. R.; Menon, M.; Thess, A.; Smalley, R. E.; Dresselhaus, G.; Dresselhaus, M. S. *Science* **1997**, *275*, 187.
(33) Burgio, L.; Clark, R. J. H. *Spectrochim. Acta, Part A* **2001**, *57*, 1491.
(34) Batonneau, Y.; Laureyns, J.; Merlin, J. C.; Brémard, C. *Anal. Chim. Acta* **2001**, *446*, 23.
(35) Vitali, G.; Rossi, M.; Terranova, M. L.; Sessa, V. *J. Appl. Phys.* **1995**, *77*, 4307.
(36) McCulloch, D. G.; Prawer, S.; Hoffman, A. *Phys. Rev. B* **1994**, *50*, 5905.
(37) Barbarossa, V.; Galluzzi, F.; Tomaciello, R.; Zanobi, A. *Chem. Phys. Lett.* **1991**, *185*, 53.
(38) Li, W.; Zhang, H.; Wang, C.; Zhang, Y.; Xu, L.; Zhu, K.; Xie, S. *Appl. Phys. Lett.* **1997**, *70*, 2684.

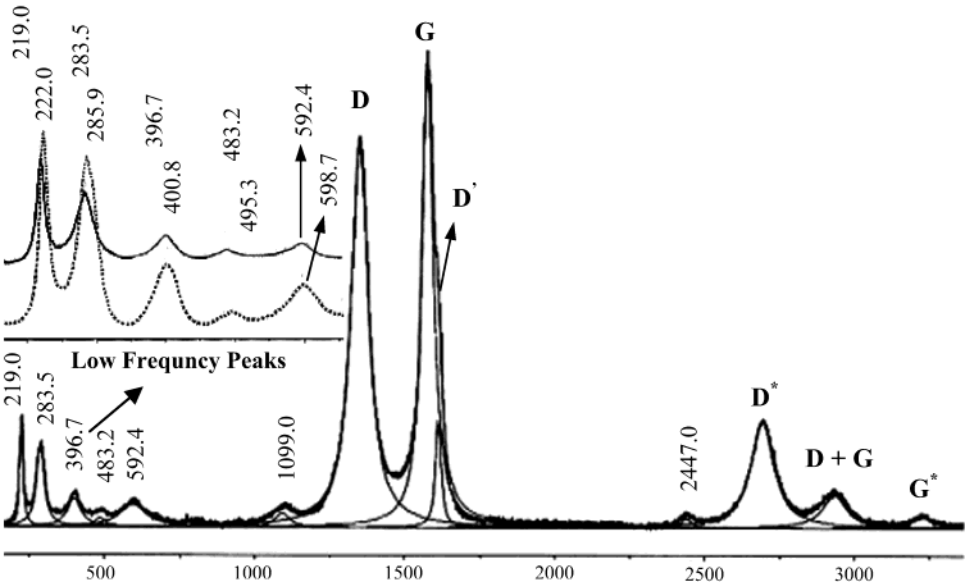

Figure 5. Raman spectrum of the pyrolysis product of the vapor mixture of pyridine and $Fe(CO)_5$ at 1050−1150 °C under a H_2 flow. The insert is the Raman spectrum comparison of Fe_2O_3 (dotted line) to the HCNT product at low frequency.

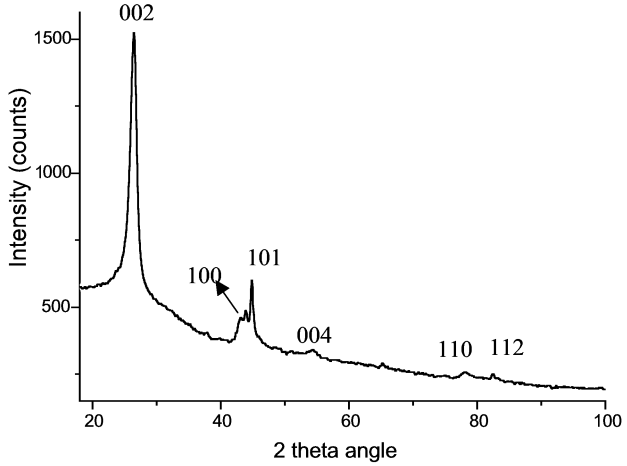

Figure 6. X-ray diffraction pattern of the pyrolysis product B of pyridine and $Fe(CO)_5$ at 1050−1150 °C under a H_2 flow.

of Raman spectra of MWNTs, but did not assign it. The second-order modes are the D* line at 2695.2 cm^{-1} (overtone of D), the combination of D and G lines at 2931.4 cm^{-1}, and the G* line at 3209.4 cm^{-1} (overtone of D′). The peak at 2447.0 cm^{-1} was frequently reported previously,[38−42] but the origin of it remains uncertain. Here, the peak 2447.0 cm^{-1} seems to be the combination of D line and the peak 1099.0 cm^{-1} (1349.9 + 1099.0 = 2448.9).

3.3. X-ray Diffraction. The WAXS pattern of product B is presented in Figure 6. The strongest peak (002) is at 26.4° (2θ). Peaks of medium intensity are (100) at 42.7° and (101) at 44.85°. The weak peaks are (004) at 54.4°, (110) at 78.15°, and (112) at 82.5° (2θ). The result shows no significant difference from the diffraction pattern of normal MWNTs.[43−44]

3.4. Growth Mechanism of HCNTs. The growth mechanism of CNTs has attracted a great deal of interest.[28,45−57] It is well accepted that the formation of CNTs is a process of metal−catalytic carbon deposition using either arc discharges[58−60] or high-temperature furnaces.[18,61−64] The metal nanoparticles serve as the catalyst for the formation of CNTs. It is generally accepted that the metal nanoparticle is in its solid state at the high temperature of CNT growth. A new view is that the catalytic metal nanoparticle is in its molten

(39) Ravindran, T. R.; Jackson, B. R.; Badding, J. V. *Chem. Mater.* **2001**, *13*, 4187.
(40) Kaster, J.; Pichler, T.; Kuzmany, H.; Curran, S.; Blau, W.; Weldon, D. N.; Delamesiere, M.; Draper, S.; Zandbergen, H. *Chem. Phys. Lett.* **1994**, *221*, 53.
(41) Hiura, H.; Ebbesen, T. W.; Tanigaki, K. *Chem. Phys. Lett.* **1993**, *202*, 509.
(42) Sun, L. F.; Liu, Z. Q.; Ma, X. C.; Zhong, Z. Y.; Tang, S. B.; Xiong, Z. T.; Tang, D. S.; Zhou, W. Y.; Zou, X. P., Li, Y. B.; Tan, K. L.; Xie, S. S.; Lin, J. Y. *Chem. Phys. Lett.* **2001**, *340*, 222.
(43) Zhou, O.; Fleming, R. M.; Murphy, D. W.; Chen, C. H.; Haddon, R. C.; Ramirez, A. P.; Glarum, S. H. *Science* **1994**, *263*, 1744.
(44) Cao, A.; Xu, C.; Liang, J.; Wu, D.; Wei, B. *Chem. Phys. Lett.* **2001**, *344*, 13.
(45) Saito, R.; Fujita, M.; Dresselhaus, G.; Dresselhaus, M. S. *Mater. Sci. Eng.* **1993**, *B19*, 185.
(46) Endo, M.; Kroto, H. W. *J. Phys. Chem.* **1992**, *96*, 6941.
(47) Smally, R. E. *Acc. Chem. Res.* **1992**, *25*, 98.
(48) Iijima, S. *Mater. Sci. Eng.* **1993**, *B19*, 172.
(49) Iijima, S.; Ichihashi, T.; Ando, Y. *Nature* **1992**, *356*, 776.
(50) Kiang, C. H.; Goddard, W. A., III *Phys. Rev. Lett.* **1996**, *76*, 2515.
(51) Endo, M.; Takeuchi, K.; Kobori, K.; Takahashi, K.; Kroto, H. W.; Sarkar, A. *Carbon* **1995**, *33*, 873.
(52) Kukovitsky, E. F.; L'vov, S. G.; Sainov, N. A.; Shustov, V. A.; Chernozatonskii, L. A. *Chem. Phys. Lett.* **2002**, *355*, 497.
(53) Louchev, O. A.; Sato, Y.; Kanda, H. *Appl. Phys. Lett.* **2002**, *80*, 2752.
(54) Lee, C. J.; Park, J.; Huh, Y.; Lee, J. Y. *Chem. Phys. Lett.* **2001**, *343*, 33.
(55) Zhang, X. X.; Li, Z. Q.; Wen, G. H.; Fung, K. K.; Chen, J.; Li, Y. *Chem. Phys. Lett.* **2001**, *333*, 509.
(56) Tsai, S. H.; Chao, C. W.; Lee, C. L.; Shih, H. C. *Appl. Phys. Lett.***1999**, *74*, 3462.
(57) Hou, H.; Schaper, A.; Weller, F.; Greiner, A. *Chem. Mater.* **2002**, *14*, 3990.
(58) Kiang, C. H.; Goddard, W. A., III; Beyers, R.; Salem, J. R.; Bethune, D. S. *J. Phys. Chem.* **1994**, *98*, 6612.
(59) Lin, X.; Wang, X. K.; Dravid, V. P.; Chang, R. P. H.; Ketterson, J. B. *Appl. Phys. Lett.* **1994**, *64*, 181.
(60) Cassell, A. M.; Screvins, W. A.; Tour, J. M. *Chem. Mater.* **1996**, *8*, 1545.
(61) Mukai, S. R.; Masuda, T.; Fujikata, Y.; Hashimoto, K. *Carbon* **1996**, *34*, 645.
(62) Guo, T.; Nikolaev, P.; Thess, A.; Golbert, D. T.; Smalley, R. E. *Chem. Phys. Lett.* **1995**, *243*, 49.
(63) Satishkumar, B. C.; Govindaraj, A.; Rao, C. N. R. *Chem. Phys. Lett.* **1999**, *307*, 158.
(64) Cheng, H. M.; Li, F.; Su, G.; Pan, H. Y.; He, L. L.; Sun, X.; Dresselhaus, M. S. *Appl. Phys. Lett.* **1998**, *72*, 3282.

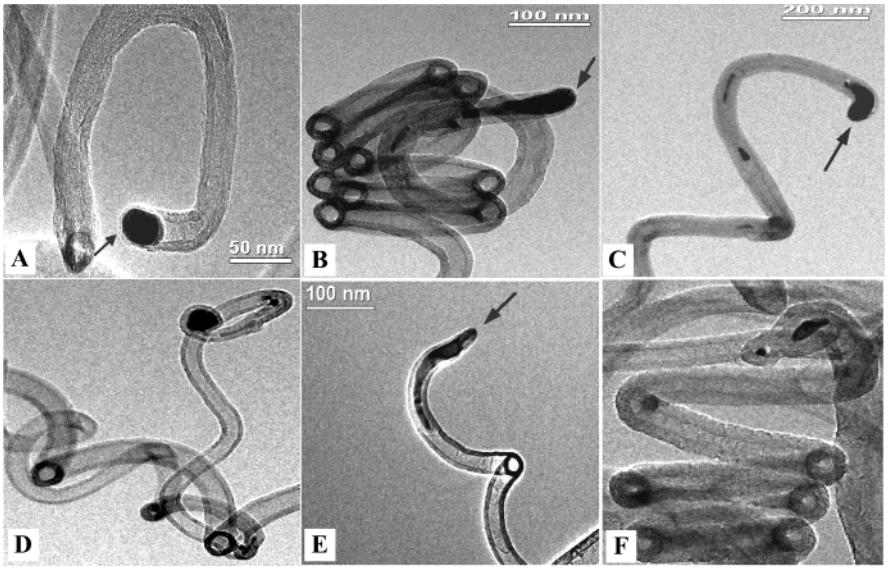

Figure 7. TEM images of various shaped metal catalyst particles at the tips of HCNTs: egg-like shape (A); taper shape (B); droplet-curved shape (C); peach shape (D); worm shape (E); and beak shape (F).

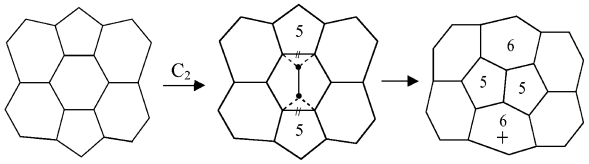

Figure 8. Scheme of a model for the insertion of a C_2 cluster to a C_6 ring with two C_5 ring neighbors on the semi-fullerene cap. The double short lines mean the connecting bond will be broken, the dotted line stands for a new connecting bond that will be formed, and the "6+" represents that the C_6 ring is a new C_6 ring formed in the C_2 absorption process.

state[52,55,65−66] at the high temperature of CNT growth. Our observation in Figure 7 shows that the shapes of iron particles at the HCNT ends are various, such as egg-like, taper, droplet-curved, peach, worm, and beak shaped, etc. It is difficult to visualize how such various shapes can form without the involvement of the liquid phase. Whether the nanoparticles are solid or liquid state at the high temperature, the iron particles are all capped by a carbon layer at the tube ends, some with a thin layer, and some with thick layers at the tip sides. We suppose that the growth point of the HCNT locates at the thin-carbon-layer side of the catalyst particle as indicated with the arrows. Those catalysts with a thick carbon layer at the tip side lost their catalytic activation, and the tubes stopped growing.

The carbon layer on the tip side of the catalyst nanoparticle seems to be a multiwalled semi-fullerene. The growth mechanism involves a carbon dimer C_2 absorption process[46,50−51,67] that is assisted by the pentagonal defects on the semi-fullerene cap. The carbon dimer C_2, which is the carbon element amount to form a unit cell of CNT and formed by the decomposition of a hydrocarbon compound (in our case, pyridine or toluene), is inserted or added in the cap consisting of

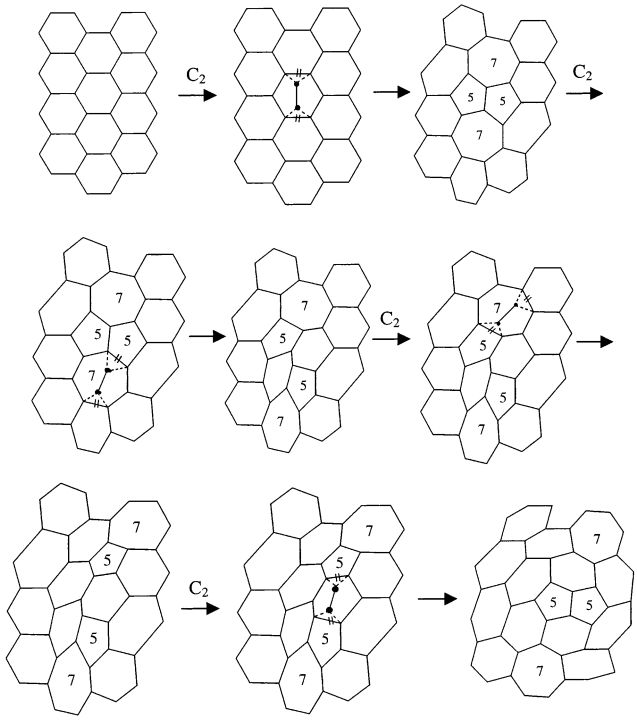

Figure 9. Scheme of a model for the insertion of a C_2 cluster to a C_6 ring without any C_5 ring neighbors to form C_5 rings and C_7 rings and how the C_5 and C_7 rings move on the semi-fullerene cap. The double short lines mean the connecting bond will be broken, and the dotted line stands for a new connecting bond that will be formed in the C_2 absorption process.

carbon hexagonal and pentagonal rings to form a new carbon hexagonal ring, which is the unit cell for the formation of CNT, as shown in Figure 8. As the sequential insertion or addition of C_2 in the cap proceeds, a straight CNT would be formed under the iron particle.

In our case, however, the CNT is helically coiled. The above mode is insufficient to explain how the helically coiled CNT was formed. As mentioned in the Introduction section, the HCNT structure is formed on the basis of the C_7 and C_5 carbon ring defects in the C_6 carbon

(65) Kukovitsky, E. F.; L'vov, S. G.; Sainov, N. A. *Mol. Mater.* **1998**, *10*, 165.
(66) Kukovitsky, E. F.; L'vov, S. G.; Sainov, N. A. *Chem. Phys. Lett.* **2000**, *317*, 65.
(67) Dresselhaus, M. S.; Dresselhaus, G.; Eklund, P. C. *Science of Fullerenes and Carbon Nanotubes*; Academic Press: New York, 1996.

ring network. Therefore, formation of the right amount of C_5 and C_7 rings in the appropriate positions is key to the formation of the HCNT structure in the synthesis of CNTs. We assume that the C_2 absorption process on the cap not only undergoes the above model but also undergoes another model under our applied high-temperature experimental condition. Here C_2 is inserted in a C_6 ring without any C_5 ring neighbor on the cap to form 2 C_5 and 2 C_7 neighbor carbon rings as shown in Figure 9. In the subsequent adsorption process, a C_2 adds to a C_7 ring to make one of the C_5-C_7 ring groups move away from another. Another insertion of C_2 to C_7 ring makes the two C_5-C_7 ring groups separate further. And then a C_2 adds to the C_6 ring between 2 C_5 rings, to make the C_5-C_7 ring group divorce and form a structure with two C_5 ring neighbors, which is similar to the structure illustrated in Figure 8. By a series of additions or insertions of C_2, the C_5 and C_7 rings move to the appropriate positions so that the "knee" structure can be formed. As a result, the helically coiled CNT is formed on a series of "knee" structures.

4. Conclusions

Large-scale synthesis of multiwalled HCNTs was accomplished by CVD pyrolysis of a vapor mixture of $Fe(CO)_5$ and pyridine or toluene at a temperature of 1050−1150 °C under H_2 flow. The diameters of HCNTs were 30−80 nm. The Raman spectrum and X-ray diffraction characterizations of HCNTs correspond well to those of normal MWNTs. The metal nanoparticles were found in various shapes at the tips of HCNTs for the catalytic growth of helically coiled tubular carbon structures, which led to the assumption that tube growth could occur by the so-called tip model. At high temperatures, the carbon dimer C_2 was supposed to be inserted or added in a hexagonal ring without any C_5 ring neighbor on the fullerene-like carbon cap to form 2 C_5 and 2 C_7 rings for the formation of HCNTs. The worm shape, taper shape, and droplet-curved shape of the nanoparticles at the ends of HCNTs suggest that the metal nanoparticle might be in its molten state at the high temperature of HCNT growth.

CM021290G